Cement & Concrete Composites 62 (2015) 146–155

Contents lists available at ScienceDirect

Cement & Concrete Composites

journal homepage: www.elsevier.com/locate/cemconcomp

Experimental and numerical characterization of the bond behavior of steel fibers recovered from waste tires embedded in cementitious matrices

Antonio Caggiano [a,b,*], Hernan Xargay [a], Paula Folino [a], Enzo Martinelli [c]

[a] LMNI, INTECIN, FIUBA, Laboratory of Materials and Structures, Faculty of Engineering, University of Buenos Aires, Argentina
[b] National Scientific and Technical Research Council (CONICET), Argentina
[c] Department of Civil Engineering, University of Salerno, Italy

ARTICLE INFO

Article history:
Received 20 April 2014
Received in revised form 16 April 2015
Accepted 25 April 2015
Available online 14 June 2015

Keywords:
Waste tires
Recycled steel fibers
FRC
Experimental characterization
Bond modeling
Pull-out

ABSTRACT

This work investigates the mechanical behavior of recycled steel fibers recovered from waste tires and, then, suitable to produce eco-friendly fiber-reinforced concrete. Particularly, the results of an experimental investigation aimed at understanding the tensile response of the aforementioned steel fibers and their bond behavior when embedded in cementitious matrices are reported and discussed. Moreover, as a case study, a fracture-based plasticity formulation for simulating the overall pull-out behavior of fibers embedded in cementitious matrices is also employed. This formulation is based on assuming a discontinuous response between interface bond stresses and the corresponding relative displacements. Then, an extensive comparison between numerical predictions and the corresponding experimental results of the pullout behavior of recycled steel fibers embedded in concrete is presented for validating and calibrating the model. A satisfactory agreement was observed between the numerical and experimental results: it demonstrates the soundness of the interface formulation.

1. Introduction

The climate change observed in the last decades and its further evolutions expected for the coming ones are the key motivation for a tremendous effort undertaken by the international scientific community to tackle some of the supposed causes of the aforementioned phenomena, such as greenhouse gas emissions and air pollution [1]. Since CO_2 emissions (and, particularly, the whole of greenhouse gases that currently define the so-called CO_{2eq}) were detected as the main reason for the above mentioned phenomena, in the last years several actions were put in place for reducing such emissions. Particularly, in the construction sector, these actions were mainly oriented to either re-using waste materials [2,3] or employing components made with renewable ones [4].

Plenty of studies on Fiber-Reinforced Concrete (FRC) addressed the feasibility of using recycled fibers, deriving from different waste streams, which can in principle play a significant role in enhancing the post-cracking response of members made of FRC [5]. Relevant applications in this field are based on employing some recycled fibers for FRC, such as tire cords/wires [6], carpet fibers [7], waste bottles PET fibers [8], waste paper fibers [9] and natural reinforcements [10].

A large amount of experimental research available in the scientific literature deals with the mechanical characterization of FRC in post-cracking response. The investigation of the mechanical performance and post-cracking response of the most common composite materials, i.e., Steel-FRC [11,12], Polypropylene FRC [13] or Hybrid-FRC [14] had been the subject of several recently issued works. Furthermore, some experimental campaigns on "eco-friendly fiber reinforced concrete composites", such as those made with either recycled steel fibers obtained from waste tires (RSFRC) [15] or natural fibers (NFRC) [16] are already available in literature.

Several theoretical models are also available and capable of simulating the failure behavior and post-cracking response of FRC at both material and structural levels. The main contributions on theoretical modeling of FRC range from empirical design relationships [17,18] to consider more complex proposals, typically based on the explicit meso-mechanical contributions of fibers on concrete cracks [19,20].

* Corresponding author at: CONICET and University of Buenos Aires, Argentina. Tel.: +54 9 11 62414876.
E-mail addresses: acaggiano@fi.uba.ar (A. Caggiano), hxargay@fi.uba.ar (H. Xargay), pfolino@fi.uba.ar (P. Folino), e.martinelli@unisa.it (E. Martinelli).

http://dx.doi.org/10.1016/j.cemconcomp.2015.04.015
0958-9465/

As a matter of principle, a sound knowledge of fiber–matrix interaction is of key importance for simulating the effect of the embedded fibers on the resulting response of structural members made out of FRC [21]. Several factors, such as fiber length, diameter, geometric details (e.g., smooth fibers, hooked-end, flattened, twisted, etc.) and materials strongly affect the FRC material response [22]. The role of fiber length and its aspect-ratio on the cracking behavior of FRC was recently pointed out by Cunha et al. [23], whereas the pull-out response of inclined fibers was investigated in Laranjeira et al. [24].

In this paper, Section 2 preliminarily describes the key geometric properties of the Recycled Steel Fibers (RSFs) employed in this research and proposes the complete definition of materials and methods. Then, the results of both direct tensile and pull-out tests are presented. Section 3 outlines the fundamental assumptions of the unified formulation for simulating the bond behavior of fibers in cementitious materials. The model was previously published by the first and fourth author in [21] with a validation focused on the debonding response of industrial steel fibers embedded in concrete matrices. However, in that work a unique softening rule was considered. Section 3.2 briefly summarizes the fracture-based model employed in this paper for simulating the inelastic debonding phenomena in RSF anchored in cementitious material. The experimental results, reported in Section 2 and some others available in literature, are then considered in Section 4 to calibrate the bond-slip model and demonstrate its ability. The influence of relevant parameters (such as fiber anchorage and diameter) is also outlined in the same section.

2. Recycled steel fibers from waste tires

A quantity of 15 kg of Recycled Steel Fibers (RSFs), a sample of which is depicted in Fig. 1, was examined to obtain a comprehensive description of both their geometry (proposed in Section 2.1) and mechanical characterization (this latter reported in Section 2.2).

It is worth mentioning that, due to the possibility that fibers could derive from different recycling plants and/or countries, it is largely accepted in the literature that a specific identification is necessary to investigate the expected variability of both geometrical and mechanical properties for the employed RSF. This is the main reason why the results of the fiber characterization obtained in the work by Aiello et al. [25] are quite different with respect to the ones obtained in this experimental campaign and discussed in the following.

Fig. 1. Recycled steel fibers employed in FRC.

2.1. Geometric characterization

As a result of the shredding and separation process, the RSFs under consideration have variable diameters and lengths, and often are characterized by irregular shapes with curls and twists. Therefore, the description of the main geometric parameters of these fibers deserves a dedicated investigation outlined this section.

First of all, fibers were cleaned and separated by some thicker pieces of steel, which were not clearly suited for being used as a spread reinforcement of FRC. Then, a detailed geometric characterization was carried out on a bunch of 2000 RSFs, randomly sampled from the available amount of RSFs. The diameter (d_f) of each single fiber was manually measured by means of a micrometer (Fig. 2): i.e., three measures were taken (i.e., at the two ends and at the fiber mid-point) and an average value was determined for each fiber. According to such measurements, the average fiber diameter was found ranging between 0.11 and 1.64 mm and characterized by a mean value of 0.27 mm. Fig. 3 highlights its apparently multimodal distribution (probably due to the mixing of different types of tires in the recycling process). However, more than one third (35.7%) of the sampled fibers exhibited an average diameter between 0.22 and 0.24 mm.

The geometric characterization of RSFs addressed also the determination of the fiber length l_f which was conventionally defined, according to the CNR-204/2006 specifications [26], as the distance between the outer ends of a fiber. Fig. 4 shows the frequency distribution of measured fiber lengths: in this case a unimodal distribution was observed (probably resulting from the unified cutting underwent during the recycling process). The mean value was of about 12 mm and almost one half of measured fiber lengths (47.1% of the total amount) was found ranging between 9 and 15 mm.

Finally, the aspect (length-to-diameter) ratio of fibers was analyzed, as it represents a key parameter controlling their mechanical performance in FRC. Fig. 5 highlights a unimodal distribution of the aspect ratio, with a mean value of about 47 and more than one half (57%) of fibers exhibited a value within the range 30–60.

2.2. Mechanical characterization

Mechanical characterization tests were carried out on RSF through tensile and pull-out tests carried out at the Laboratory of Materials and Structures (LAME) of the University of Buenos Aires (Argentina).

2.2.1. Direct tensile test

Direct tensile tests were carried out in displacement control by means of an electromechanical dynamometer "Instron Dynamometer 4467". During the tests a proper anchorage within the grips was considered in order to avoid possible failure in this zone.

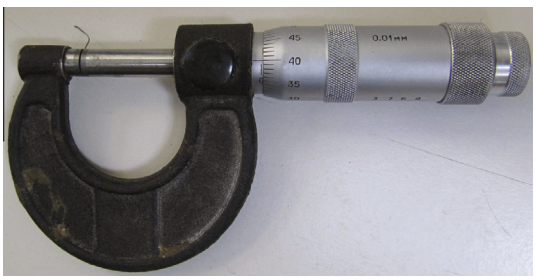

Fig. 2. Characterization of fibers: diameter measurement by a micrometer.

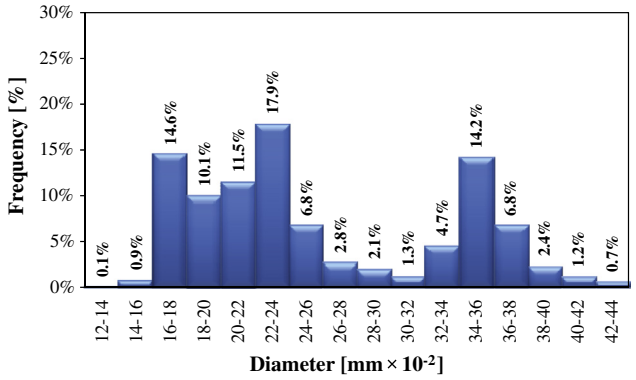

Fig. 3. Frequency of diameter measurements.

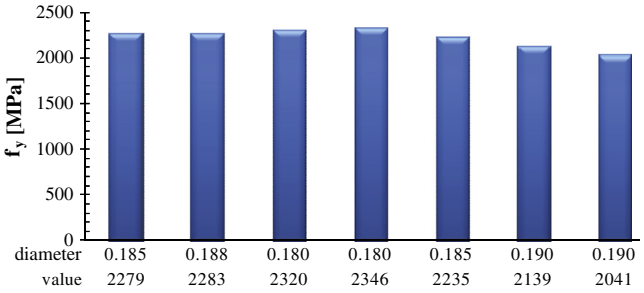

Fig. 6. Tensile strength of RSF.

The fiber tensile strength, f_y, was evaluated as

$$f_y = \frac{4P_{\max}}{\pi d_{f,m}^2} \quad (1)$$

where $P_{\max}$ is the maximum registered load while $d_{f,m}$ is the average value of fiber diameters.

The results of the tensile tests performed on seven fibers with similar diameters are reported in Fig. 6. The average value and the relative standard deviation of these results are, 2235 MPa and 4.86%, respectively. The experimental results are in good agreement with available test data on RSF by Aiello et al. [25] and demonstrate that tensile strength of RSF is comparable to classical values of industrial steel fibers [27].

2.2.2. Pull-out test

Pull-out tests on single RSFs are described in this section. The materials used in the composition of the surrounding concrete, designed to reach a target 28 days mean cubic compressive strength of 40 MPa, were: cement CEM II/A-LL 42.5R type, three types of crushed limestone aggregates (the N1 type characterized by coarse natural aggregates with grain size ranging between 2 and 10 mm, N2 with grain size from 10 to 20 mm and sand) according to EN-12620 [28] and UNI-110392-1 [29], a constant cement content of 320 kg/m^3, a free water to-cement-ratio w/c of 0.51 and superplasticizer.

Cubic concrete specimens (size 100 mm) were used for pull-out tests in which a single RSF was centrally embedded. The single-sided specimen was mounted in a supporting steel system fixed to the testing machine frame. Then, the protruding end of the steel fiber was fastened to a standard grip which allowed a secure hold of the fiber. The pull-out test was realized at approximately 28 days after concrete casting and performed with a servo-hydraulic "Instron Dynamometer 4467" machine with a capacity of 250 kN under displacement control.

The same type of RSFs tested in direct tension, with an average diameter of 0.185 mm, was tested in pull-out in order to evaluate the bond-slip response. Two different values of embedded fiber length were examined: i.e., 20 and 40 mm. The number of specimens examined for each embedded length was 5.

The results, reported in terms of load–displacement curves, highlights the influence of the embedded length on the fiber-to-concrete interface failure, as can be seen in Figs. 7 and 8, corresponding to an embedded length of 20 and 40 mm, respectively.

The initial part in each curve, corresponding to the stretching of the fibers, was accurately cleaned. All specimens with equal anchorage length exhibited a similar behavior in terms of bond-slip response.

Two distinct failure modes clearly emerge from the depicted force-slip curves. On the one hand, Fig. 7 deals with specimens with an embedded length of 20 mm in which the fiber-to-concrete specimens failed in debonding mechanism. A linear behavior up to the peak strength can be observed, then, after that peak, a softening zone can be observed with a gradual loss of bonding. On the other hand, all fibers with embedded lengths of 40 mm (Fig. 8) failed in tension: it means that the ultimate stress of the fibers is attained before that the peak load was ideally reached under pull-out.

Furthermore, if the experimental results in Fig. 7 are compared against pull out tests corresponding to Industrial Steel Fibers (ISFs) [30], substantial differences can be observed from a quantitative viewpoint. On the one hand, the mean peak load in pull-out tests of ISF is about two to ten times the maximum one obtained

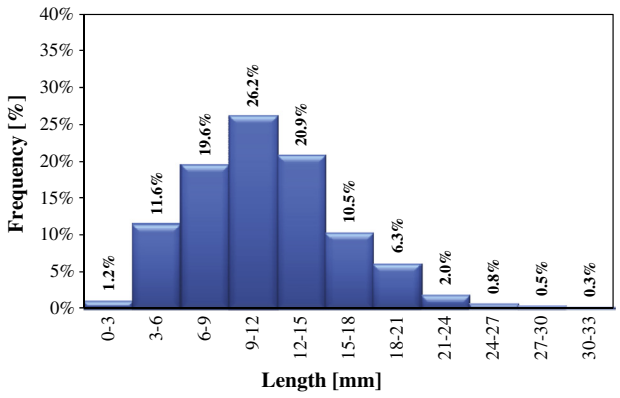

Fig. 4. Frequency of fiber length measurements.

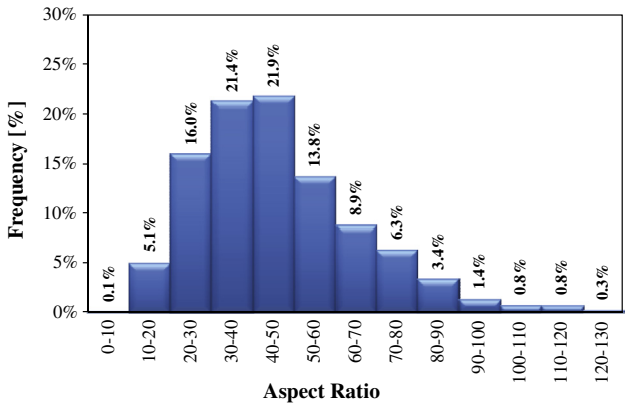

Fig. 5. Frequency of the aspect ratio.

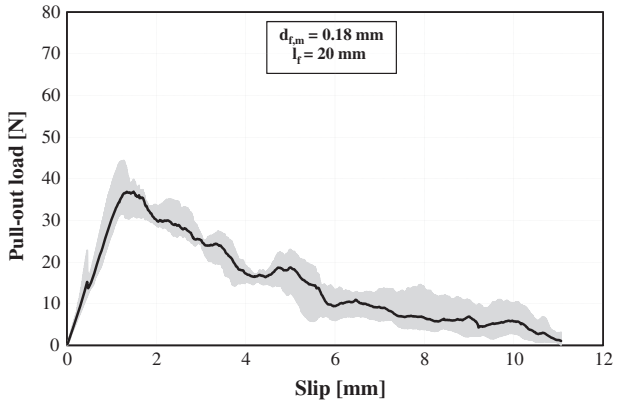

Fig. 7. Applied load vs. slip (embedded length of 20 mm).

for RSF, considering similar embedded lengths. Nevertheless, even though RSFs are characterized by smaller diameters than ISFs, both fibers lead to bond strengths of the same magnitude. On the other hand, slip corresponding to the peak load for ISF is about one hundred times smaller than the mean 2 mm slip that can be registered in RSF-to-concrete debonding. Thus, these results mean that RSFs need a greater crack opening to be pulled out and, consequently, it seems that these fibers did not contribute to reduce the crack width, although they could enhance the post-peak toughness and ductility.

Pullout tests proposed in this work were performed with the aim of obtaining the bond parameters which characterize the RSF-concrete interface response. The obtained bond behavior was employed for calibrating the interface shear-slip model for simulating the entire pull-out response of RSFs embedded in a cementitious matrix. It is worth mentioning that, since the pullout tests of RSF are not standardized, the embedded length was defined by the authors. As a matter of fact, only a few papers in the literature proposed some procedures in this field. However, determining the "critical length" resulting in the transition from debonding to tensile failure of RSF was one of the first objectives of the study: since all 40 mm specimens failed in tension and all 20 mm ones exhibited a debonding crisis, it was clear that this critical length was somehow intermediate between the two aforementioned values. Even if further experimental works are needed with the aim of extending the pull-out behavior to other aspect ratios, the obtained data allowed to calibrate the interface model as proposed in the following sections. Therefore, the results obtained from the specimens with the shorter embedment length were employed for calibrating the model that was, then, employed for simulating the "structural" behavior of specimens with variable embedments.

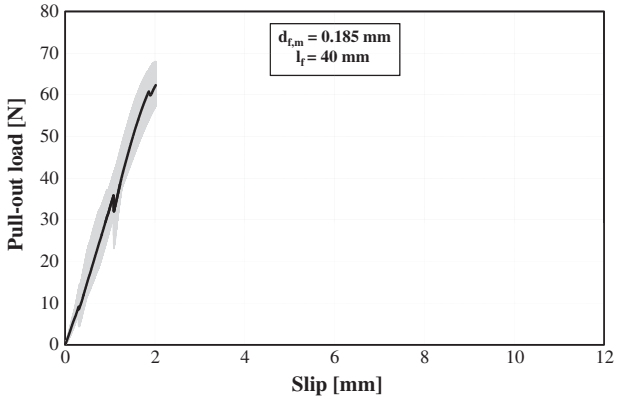

Fig. 8. Applied load vs. slip (embedded length of 40 mm).

3. Pull-out mechanisms of fiber-to-concrete: basic assumptions

Since the present work was specifically aimed at presenting an application of the interface shear-slip model for simulating the entire bond-slip response of RSFs embedded in concrete matrix, it focused on the key parameters for obtaining the numerical solution in terms of pull-out loads versus the applied slips. For the sake of simplicity, the cementitious matrix was actually considered as a rigid body, while all non-linearities were lumped at the interface between fiber and surrounding concrete. The behavior of the RSF was considered as elastic perfectly plastic materials.

Therefore, the following main assumptions of such modeling are proposed:

- RSFs, characterized by a linear elastic perfectly plastic behavior, was modeled by employing one-dimensional two-nodes isoparametric truss elements (to see Section 3.1);
- The interface slip between RSF and the surrounding concrete matrix was modelled by means of interface elements as shown in Fig. 9: the constitutive relationship, considered for modeling the non-linear response of the fiber-to-concrete joints, adopted the fracture-based plasticity model presented in Section 3.2;
- Neglecting the strains in the surrounding concrete, the cementitious matrix was ideally considered as a rigid block (no strains occurred in this zone).

3.1. Behavior of steel fibers

The mechanical behavior of the recycled steel fibers was modeled as a 1-D linear elastic perfectly plastic material. The incremental stress–strain law can be written as

$$\dot{\sigma}_f = E_f^{ep}\dot{\varepsilon}_f \tag{2}$$

being $\dot{\sigma}_f$ the axial stress rate of the fiber, $\dot{\varepsilon}_f$ the incremental axial strain and the tangent elasto-plastic modulus E_f^{ep} takes the following two distinct values

$$\begin{cases} E_f^{ep} = E_f & \textit{elastic/unloading} \\ E_f^{ep} = 0 & \textit{loading with } \dot{\lambda}_f > 0 \end{cases} \tag{3}$$

where $\dot{\lambda}_f$ is the non-negative plastic multiplier captured by means of the Kuhn–Tucker loading condition and E_f represents the uniaxial elastic module of the fiber.

Finally, the yielding criterion takes the following expression

$$f_f = |\sigma_f| - \sigma_{y,f} \leqslant 0 \tag{4}$$

in which $\sigma_{y,f} \geqslant 0$ is the yield limit of the steel.

3.2. Fracture-based interface constitutive model

A big number of theoretical models for interface elements (more of them available in commercial finite element codes) are based on assuming "a priori" a bond-slip law (either bi-linear, three-linear or generally non-linear in shape) for simulating the behavior of the adhesive interface. On the contrary, the model proposed by the authors is fully developed within the physically sound framework of the "Flow Theory of Plasticity". Particularly, the elastic response of a generic point on the fiber interface is described by a linear branch up to a given threshold value of the bond stress; then, the fracture propagation and the corresponding stress release process is simulated through general non-linear softening relationships, though assuming that fracture develops in mode II. The formulation proposed in this form is able to correctly predict the irreversible nature of the plastic phenomenon during bond-slip response.

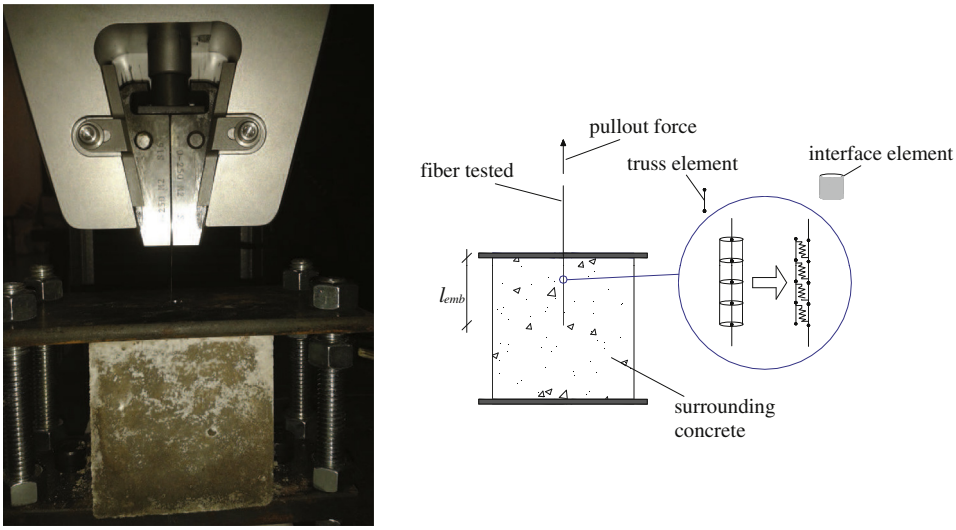

Fig. 9. Pull-out specimen: (a) test set-up and (b) the corresponding considered FE schematization.

The rate-independent contact law is highlighted in this section with the purpose of simulating the fiber-to-concrete debonding under pull-out loading. Particularly, the bond-slip model was directly implemented as plasticity-type constitutive law for interface elements.

In the framework of the classical flow theory of plasticity, the following incremental basic equations were employed

$$\dot{s} = \dot{s}^e + \dot{s}^p \quad \dot{s}^e = \frac{\dot{\tau}}{k_E} \quad \dot{\tau} = k_E(\dot{s} - \dot{s}^p) \tag{5}$$

being $\dot{s}$ the rate of the relative joint slip, which can be decomposed into an elastic and a plastic component, $\dot{s}^e$ and $\dot{s}^p$, respectively. The elastic stiffness is represented by the modulus k_E while $\dot{\tau}$ is the rate of interface shear stress.

According to the classical flow rule, the inelastic slip rate is defined as follows

$$\dot{s}^p = \dot{\lambda}\frac{\partial f}{\partial \tau} \tag{6}$$

where $\dot{\lambda}$ is the non-negative plastic multiplier which was derived by means of the classical consistency loading/unloading conditions. They assume the following expressions (also known as Kuhn–Tucker relationships)

$$\dot{\lambda} \geqslant 0, \quad f \leqslant 0, \quad \dot{\lambda} f = 0, \quad \dot{\lambda}\dot{f} = 0 \tag{7}$$

in which $f = f(\tau, \tau_y)$ describes the considered elastic domain

$$f(\tau, \tau_y) = \tau^2 - \tau_y^2 \leqslant 0 \tag{8}$$

where τ_y represents the yielding shear stress.

The variation in τ_y is assumed to be linear in terms of the following expression

$$\tau_y = \tau_{y,0}(1 - \psi) \tag{9}$$

where $\tau_{y,0}$ is the shear strength, given as material parameter of the model, while ψ is a scaling function defined by Carol et al. [31] as follows

$$\psi(\xi) = \frac{e^{-\alpha}\xi}{1 + (e^{-\alpha} - 1)\xi} \tag{10}$$

where $\xi = w_{sl}/G_f$, being G_f the available fracture energy in pure Modes II.

The parameter w_{sl}, which actually measures the evolution of the material parameter τ_y in softening range, represents the work spent during the interface fracture (bond-slip) process. It is expressed in the following rate form

$$\dot{w}_{sl} = \tau \cdot \dot{s}^p \tag{11}$$

Then, the total dissipated work is obtained by integrating the fracture work increments during the delamination process.

The softening parameter α of Eq. (10) provides a series of descending softening curves as shown in Fig. 10. Particularly, when $\alpha = 0$, after stress integration at Gauss-point, the interface model leads to the well-known exponential negative softening $\tau - s$ law [21].

The classical elasto-plastic rate equations can be obtained by combining the constitutive Eq. (5) and the consistency condition of Eq. (5)

$$\dot{f} = \frac{\partial f}{\partial \tau}\dot{\tau} + \frac{\partial f}{\partial \lambda}\dot{\lambda} \tag{12}$$

where the softening parameter $H = -\frac{\partial f}{\partial \lambda}$ is derived as follows

$$H = -\frac{\partial f}{\partial \lambda} = -\frac{\partial f}{\partial \tau_y}\frac{\partial \tau_y}{\partial w_{sl}}\frac{\partial w_{sl}}{\partial s^p}\frac{\partial f}{\partial \tau}. \tag{13}$$

The classical expression for the rate of the tangential stiffness, k^{ep}, is obtained by combining and solving Eqs. (12) and (13)

$$k^{ep} = k_E\left(1 - \frac{\left(\frac{\partial f}{\partial \tau}\right)^2 k_E}{H + k_E\left(\frac{\partial f}{\partial \tau}\right)^2}\right). \tag{14}$$

The model was finally implemented by defining the algorithmic tangent operator with the linearized tangential format of the incremental shear-slip law. Further details about the above mentioned integration algorithms can be found in Caggiano and Martinelli [21].

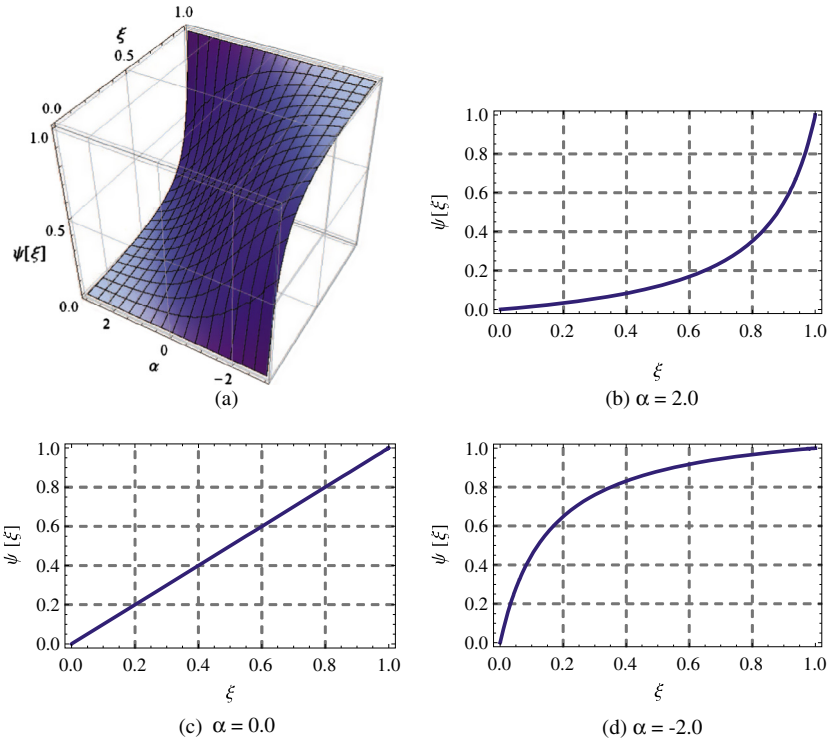

Fig. 10. Softening law provided by Eq. (10): (a) tridimensional plot and two-dimensional curves when (b) $\alpha = 2.0$, (c) $\alpha = 0.0$ and (d) $\alpha = -2.0$.

4. Numerical simulations

4.1. Comparison between numerical simulations and experimental results

Numerical analyses were performed for simulating the mechanical behavior observed in pull-out tests on RSFs embedded in cementitious matrices.

The numerical analyses were performed by means of a FE code implemented by the authors and referring to the main geometric and material properties deduced by the experimental evidences. In order to have a wide spectrum of experimental results, the test results highlighted in Section 2 and that ones reported in the work by Aiello et al. [25] were considered as reference for calibrating the interface model for RSF-to-concrete joints. Then, numerical pull-out tests were performed by considering different embedded lengths, while the input data characterizing each one of the two sets of considered experimental campaign were not altered.

Three different fiber anchoring lengths were considered: i.e., $l_{emb} = 15$ mm, 20 mm and 40 mm, and two fiber diameters, $d_f = 0.18$ and $d_f = 0.25$ mm, respectively. For the first analyzed case, RSFs, having a mean tensile strength of 2235 MPa, a module of elasticity of 200 GPa and a mean diameter of 0.18 mm, were considered in the simulation.

For the numerical simulation of the RSF-to-concrete pull-out by Aiello et al. [25], a mean tensile strength of 2314 MPa, a module of elasticity of 200 GPa and a mean diameter of 0.25 mm were considered.

The experimental results obtained from specimens with the shorter embedment length were employed for calibrating the model parameters. Particularly, the elastic stiffness k_E of the $\tau - s$ law was derived by writing the classical mechanical equations of "equilibrium", "compatibility" and "stress–strain relationships" as explained by [32]. Therefore, the following implicit expression was obtained for determining the value of k_E

$$k_E = \frac{\alpha_1}{\pi \tanh(\alpha_1 l_{emb}) d_f} \frac{F_{50}}{s_{50}} \tag{15}$$

where $\alpha_1 = 2\left(\frac{k_E}{d_f E_f}\right)^{1/2}$, while s_{50} and F_{50} are, respectively, the slip and the pullout force recorded at the end of the (idealized) elastic range of the experimental response observed in the pull-out tests.

Furthermore, for short embedment lengths, the assumption of uniform bond stress mobilized throughout the fiber can be reasonable and, hence, medium and maximum values of the bond-slip distribution are coincident. This assumption leads to calibrating the interface bond strength $\tau_{y,0}$ as follows

$$\tau_{y,0} = \frac{F_{\max}}{\pi d_f l_{\text{emb}}} \tag{16}$$

being F_{max} the maximum pullout load observed in the experimental test. Finally, in case of short embedments the (unit) fracture energy in pure mode II, G_f, can be obtained by means of the following approximate expression

$$G_f = \frac{\int_0^\infty F(s)\,\mathrm{ds}}{\pi d_f l_{\text{emb}}} - \frac{\left(\frac{F(s)}{\pi d_f l_{\text{emb}}}\right)^2}{2\,k_E} \tag{17}$$

where $\int_0^\infty F(s)\,ds$ represents the inelastic portion of the enclosed area of the experimental F–s curve and can be calculated by transforming the integral into a discrete summation.

Thus, the values of the relevant material parameters, identified for the numerical tests and based on the shorter tests of the two experimental campaigns, considered in the present paper, are:

- experimental campaign (Section 2): $k_E = 2.50$ MPa/mm, $\tau_{y,0} = 3.25$ MPa, $G_f = 21$ N/mm and $\alpha = 0.00$;
- experimental campaign by Aiello et al. [25]: $k_E = 4.31$ MPa/mm, $\tau_{y,0} = 6.80$ MPa, $G_f = 32$ N/mm and $\alpha = 0.25$.

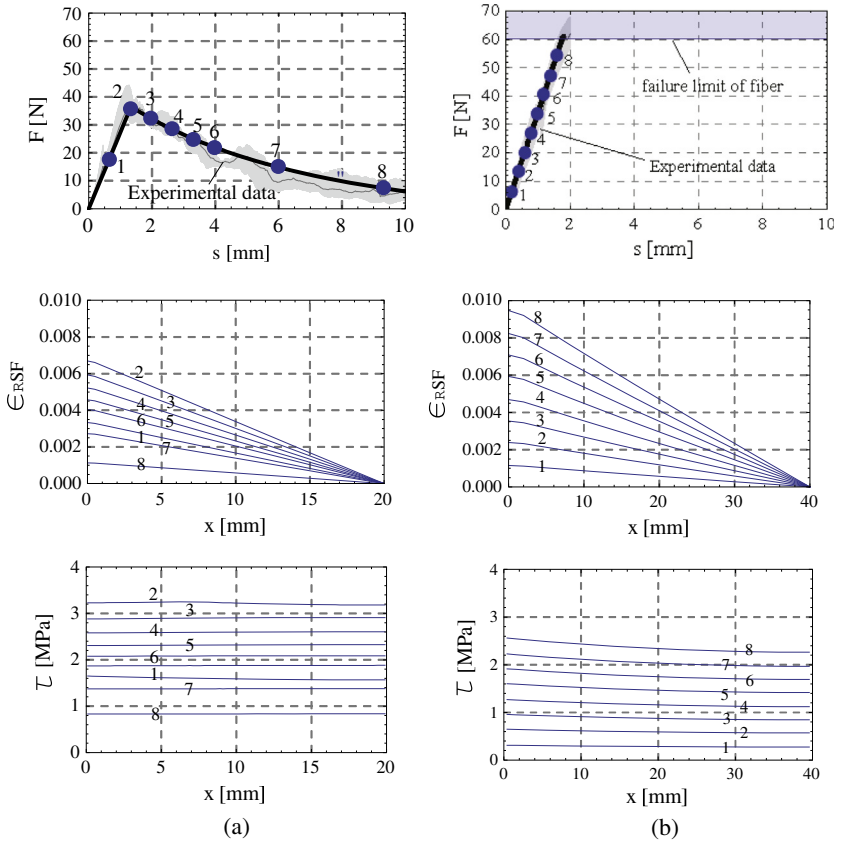

Fig. 11. Force (F) – slip (s) relationship at the loaded end, axial strain (ϵ_{RSF}) distributions and interface shear stresses (τ): numerical simulation against experimental data for (a) $l_{emb} = 20$ mm and (b) $l_{emb} = 40$ mm.

It is worth highlighting that the mechanical behavior of concrete under different load scenarios is strongly influenced by the actual concrete quality [33,34]. Pull out behavior is not an exception: the bond strength depends not only on the characteristics of RSFs, but also on the quality of the concrete matrix. Thus, parameters characterizing the bond-slip response of RSFs embedded in a concrete matrix are affected by the coupling of fibers and concrete. Particularly, as regards the concrete quality, the two sets of experimental results presented in the paper corresponds to concrete with different uniaxial compressive strengths, namely equal to 40 MPa and 50 MPa, for the tests carried out by the authors and for the ones presented by [25], respectively. Therefore, it is obvious that the two sets of test results can only be reproduced by considering different parameters within the model considered in the paper.

After a preliminary sensitivity analysis, the number of rod elements and IEs adopted in the FE model to represent fiber and interface, respectively, was 50 for all cases.

The calibration procedure assumes that different interface properties were assumed in the constitutive law described in Section 3.2 for the two experimental campaigns (namely, the one carried out by the authors and that one reported by Aiello et al. [25]). This assumption derives from the difference of the mechanical properties of the concrete substrate which characterizes each campaign. However, the predictive capacity of the proposed model is demonstrated by the significant level of accuracy obtained in such comparisons by assuming only one set of values for the relevant fracture-related parameters, while different embedded lengths are evaluated. As a matter of fact, since RSFs are not produced via a standard industrial process, their geometric and mechanical properties can be significantly variable as a result of different recycling procedures. Consequently, the bond behavior can also be affected by such a variability and, in principle, the numerical values of the relevant fracture-related parameters should be calibrated for each set of fibers, as it was done in this work.

The comparison between the load-slip experimental behavior against the numerical predictions is highlighted in Figs. 11 and 12. Numerical simulations are in acceptable agreement with results observed in all pull-out tests. Both experimental and numerical results show that the increase in pull-out strength is directly related to the anchoring lengths (from 20 to 40 mm in Fig. 11 and from 15 to 20 mm in Fig. 12) and fiber diameters (i.e., considering $d_f = 0.18$ mm and $d_f = 0.25$ mm). As a matter of fact, the proposed procedure well captures the effects of both parameters.

It is worth highlighting that the rather satisfactory agreement between experimental results and numerical simulations is based on employing the same set of input parameters (which differ from one to other for the two considered experimental campaigns) needed by the numerical model for describing both elastic (approximately up the peak load) and fracture (softening) response of the RSF tested under pull-out. Furthermore, the model proposal correctly predict the case in which the fiber fails in tension (not for debonding mechanism). This is the case of fiber which were embedded for 40 mm in the concrete block.

The detailed simulation and overall response of the complete debonding processes, developing in the four cases, is described in Figs. 11 and 12. The fiber-to-concrete shear stress and strain distributions throughout the bond length were obtained by numerical simulations. In particular, the distribution of interface shear stresses throughout the bond length refers to several force/slip levels

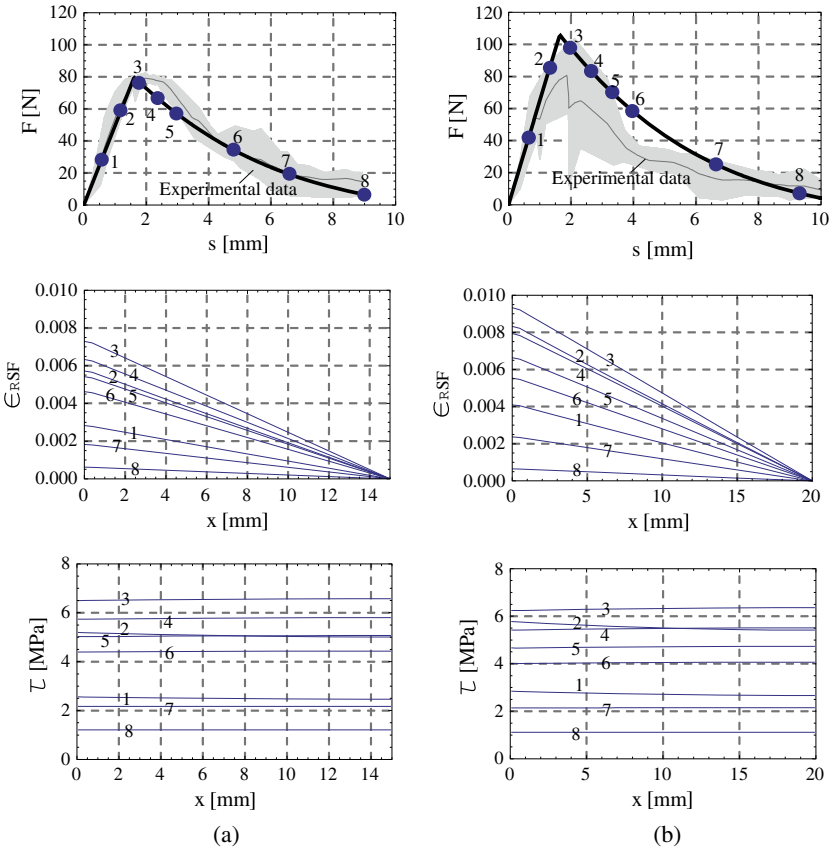

Fig. 12. Force (F) – slip (s) relationship at the loaded end, axial strain (ϵ_{RSF}) distributions and interface shear stresses (τ): numerical simulation against experimental data by [25] for (a) $l_{emb} = 15$ mm and (b) $l_{emb} = 20$ mm.

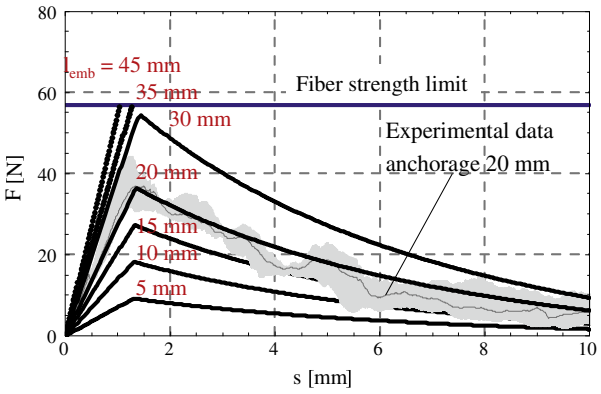

Fig. 13. Effect of the bond length on the force (F) – slip (s) relationship at the loaded end.

labeled by the dots reported in the F–s curves. Figs. 11 and 12 also highlight the axial strain distribution, namely $\varepsilon_s[x] = \frac{ds}{dx}$, at each considered abscissa x of the analyzed recycled steel reinforcement tested under pull-out: each curve refers at several force levels mentioned on the F–s curves.

Figs. 11 and 12 show that both the experimental tests and the numerical results based on the proposed numerical approach, indicate that a greater anchoring length of the fibers improves the resulting mechanical behavior under pull-out load. Nevertheless, the results of Fig. 12b by Aiello et al. [25] outline that the pull-out test with the anchorage length of 20 mm was characterized by a greater dispersion than those obtained for 15 mm of embedment length. This fact probably explains why the numerical results, based on the zero-thickness interface model, show a good agreement only with the most favorable experimental results, especially for the case of $l_{emb} = 20$ mm.

4.2. Predictive numerical results

This section reports the results of a parametric analysis carried out for simulating the pull-out tests through the fracture-based interface presented in Section 3.2. For this purpose, different numerical tests were performed, each one of them corresponding to a given embedded length, while the calibrated parameters obtained in the above subsection are employed in this parametric study, for all cases.

Fig. 13 highlights the load-slip curves obtained by adopting the same model parameters and assuming the embedded length as a unique variable for the numerical simulations $l_{emb} = 20$ mm and l_{emb}. It is clearly evident that, increasing the bond anchorage, the initial elastic stiffness as well as the maximum load tend to increase. Furthermore, it is worth observing that for a certain bond length (between embedments of 30–35 mm), a change of failure mode occurs: from the classical failure under debonding, whose response is characterized by a load vs. slip softening response, to tensile failure of fibers. Based on Fig. 13, it is possible to define an effective bond length, namely a possible threshold anchorage, beyond which the maximum load is equal to the following value

$$F_t = \frac{d_f^2}{4}\pi\sigma_{y,f} \tag{18}$$

being d_f and $\sigma_{y,f} \geqslant 0$ the diameter and the yield limit of the fiber, respectively.

5. Conclusions

The results of an experimental campaign aimed at characterizing both the tensile and bond behavior of recycled steel fibers recovered from waste tires are presented in this paper. Then, the work reports a fracture-based formulation for describing the overall pull-out response of recycled steel fibers embedded in cementitious matrices. A series of final remarks can be drawn out on the basis of both the model formulation and the proposed applications:

- Although several theoretical models are already available in the scientific literature, based on non-linear bond-slip relationships chosing "a priori" to simulate the interface bond between fibers to concrete, this work provides readers with a more general formulation based on key "Flow Theory of Plasticity" principles enhanced with fracture energy concepts for the post-peak response.
- The description of the complete incremental plasticity-based formulation of the model was reported and the key aspects of the numerical procedure needed for handling such a relationship were outlined.
- Model performances demonstrate a rather good agreement between experimental results and numerical simulations based on the same set of input parameters needed by the interface numerical model for describing both the elastic and fracture response of the recycled steel fibers anchored in concrete.

It is worth highlighting that the discontinuous-based unified formulation can be directly employed in theoretical models aimed at simulating the behavior of FRC through discrete-crack approaches, as such models (i.e., meso-mechanical ones) explicitly simulate the bond-slip response of fibers embedded in cementitious matrices. In principle, the proposed model in its present form is only restricted to simulate the pull-out behavior of fibers embedded in cementitious composites with no fiber inclination. The interaction effects between inclined fibers and surrounding concrete which take place in terms of local inelastic deformations of the fiber, lateral pressure imposed onto the substrate and the local inelastic damage of concrete will be accounted in future extension of the present formulation.

Pull-out test results are employed in this work to calibrate the bond-slip numerical model which can be used in the frame of a meso-mechanical approach for fiber reinforced cementitious composites previously proposed [19,35]. In that approach, fiber bridging effects, are formulated in terms of two main (and separated) mechanisms: the bond-slip, theoretically approached as outlined in this work while typical failures characterized by local crushing of the surrounding matrix due to transversal mechanisms of fibers crossing the crack is considered through an appropriate constitutive model. The adoption of the presented formulation within the framework of general meso-mechanical models of FRC is, at the same time, the key motivation and the most relevant development of the present research.

As a final comment, it is highlighted that recycled fibers considered in this work seem to be suitable to be used for obtaining cementitious composites with enhanced ductility and toughness properties. Nevertheless, further researches are still needed for characterizing the durability properties of RSFs against the degradation phenomena possibly triggered by their exposure to aggressive environment.

Acknowledgements

The present study is part of the activities carried out by the Authors within the "EnCoRe" Project (FP7- PEOPLE-2011-IRSES n. 295283; www.encore-fp7.unisa.it) funded by the European Union within the Seventh Framework Programme. "RPN Tyres S.r.l" is also acknowledged for having supplied the Recycled Steel Fibers for the experimental campaign. A special acknowledgment goes also to Mr. Victor Vega for the great collaboration in the experimental activity carried out at the Laboratory of Structures of the University of Buenos Aires. Finally, the collaboration to the geometric characterization of the recycled steel fibers offered by Mr. Giuseppe Ferrara and Mr. Danilo Flora, as part of their B.Sc. projects at the University of Salerno, is also acknowledge.

References

[1] P. de Wilde, D. Coley, The implications of a changing climate for buildings, Build Environ 55 (0) (2012) 1–7.
[2] V. Mymrin, S. Correa, New construction material from concrete production and demolition wastes and lime production waste, Constr Build Mater 21 (3) (2007) 578–582.
[3] P. Folino, H. Xargay, Recycled aggregate concrete – mechanical behavior under uniaxial and triaxial compression, Constr Build Mater 56 (0) (2014) 21–31.
[4] M.M. Johari, A. Zeyad, N.M. Bunnori, K. Ariffin, Engineering and transport properties of high-strength green concrete containing high volume of ultrafine palm oil fuel ash, Constr Build Mater 30 (0) (2012) 281–288.
[5] Y. Wang, H. Wu, V.C. Li, Concrete reinforcement with recycled fibers, J Mater Civ Eng 12 (4) (2000) 314–319.
[6] H.C. Wu, Y.M. Lim, V.C. Li, Application of recycled tyre cord in concrete for shrinkage crack control, J Mater Sci Lett 15 (20) (1996) 1828–1831.
[7] Y. Wang et al., Utilization of recycled carpet waste fibers for reinforcement of concrete and soil, Recycl Textiles (2006) 213–224.
[8] D. Foti, Preliminary analysis of concrete reinforced with waste bottles pet fibers, Constr Build Mater 25 (4) (2011) 1906–1915.
[9] P. Soroushian, Z. Shah, J.P. Won, Optimization of wastepaper fiber–cement composites, ACI Mater J 92 (1) (1995).
[10] A. Grozdanov, M. Avella, A. Buzarovska, G. Gentile, M.E. Errico, Reuse of natural fiber reinforced eco-composites in polymer mortars, Polym Eng Sci 50 (4) (2010) 762–766.
[11] S. Singh, S. Kaushik, Fatigue strength of steel fibre reinforced concrete in flexure, Cem Concr Compos 25 (7) (2003) 779–786.
[12] E. Toussaint, J.F. Destrebecq, M. Grdiac, A detailed study of crack propagation in cement-based fibre composite beams under bending, Cem Concr Compos 27 (3) (2005) 399–411.
[13] M. Elser, E. Tschegg, S. Stanzl-Tschegg, Fracture behaviour of polypropylene-fibre-reinforced concrete under biaxial loading: an experimental investigation, Compos Sci Technol 56 (8) (1996) 933–945.
[14] N. Banthia, F. Majdzadeh, J. Wu, V. Bindiganavile, Fiber synergy in hybrid fiber reinforced concrete (hyfrc) in flexure and direct shear, Cem Concr Compos 48 (0) (2014) 91–97.
[15] A.G. Graeff, K. Pilakoutas, K. Neocleous, M.V.N. Peres, Fatigue resistance and cracking mechanism of concrete pavements reinforced with recycled steel fibres recovered from post-consumer tyres, Eng Struct 45 (0) (2012) 385–395.
[16] F. de Andrade Silva, B. Mobasher, R.D.T. Filho, Fatigue behavior of sisal fiber reinforced cement composites, Mater Sci Eng: A 527 (21–22) (2010) 5507–5513.
[17] M. Nataraja, N. Dhang, A. Gupta, Stress-strain curves for steel-fiber reinforced concrete under compression, Cem Concr Compos 21 (56) (1999) 383–390.
[18] A. Brandt, M. Glinicki, J. Potrzebowski, Application of FRC in construction of the underground railway track, Cem Concr Compos 18 (5) (1996) 305–312.
[19] A. Caggiano, G. Etse, E. Martinelli, Zero-thickness interface model formulation for failure behavior of fiber-reinforced cementitious composites, Comput Struct 9899 (0) (2012) 23–32.
[20] V.M. Cunha, J.A. Barros, J.M. Sena-Cruz, A finite element model with discrete embedded elements for fibre reinforced composites, Comput Struct 94–95 (0) (2012) 22–33.
[21] A. Caggiano, E. Martinelli, A unified formulation for simulating the bond behaviour of fibres in cementitious materials, Mater Des 42 (0) (2012) 204–213.
[22] B. Banholzer, W. Brameshuber, W. Jung, Analytical evaluation of pull-out teststhe inverse problem, Cem Concr Compos 28 (6) (2006) 564–571.
[23] V. Cunha, J. Barros, J. Sena-Cruz, Pullout behavior of steel fibers in self-compacting concrete, ASCE – J Eng Mech 22 (1) (2010) 1–9.
[24] F. Laranjeira, C. Molins, A. Aguado, Predicting the pullout response of inclined hooked steel fibers, Cem Concr Res 40 (10) (2010) 1471–1487.
[25] M.A. Aiello, F. Leuzzi, G. Centonze, A. Maffezzoli, Use of steel fibres recovered from waste tyres as reinforcement in concrete: pull-out behaviour, compressive and flexural strength, Waste Manage 29 (6) (2009) 1960–1970.
[26] CNR-204/2006. CNR Consiglio Nazionale delle Ricerche: Istruzioni per la progettazione, l'esecuzione ed il controllo di strutture di calcestruzzo fibrorinforzato; 2006 [in Italian].
[27] Officine-Maccaferri. Cold drawn steel wire fibre, for concrete reinforcement. TECHNICAL DATA SHEET, WIRAND FIBRE FS7; 2010.
[28] UNI-EN-12620. Aggregates for concrete, volume Ref. No. EN 12620:2002 E. Europ. Committee for Standardization, Brussels; 2002.

[29] UNI-11039-1. Steel fibre reinforced concrete – Definitions, classification and designation. UNI Editions, Milan, Italy; 2003.
[30] J. Shannag, R. Brincker, W. Hansen, Pullout behavior of steel fibers from cement-based composites, Cem Concr Res 27 (1997) 925–936.
[31] I. Carol, P. Prat, C. Lopez, Normal/shear cracking model: applications to discrete crack analysis, ASCE – J Eng Mech 123 (1997) 765–773.
[32] A. Caggiano, E. Martinelli, C. Faella, A fully-analytical approach for modelling the response of {FRP} plates bonded to a brittle substrate, Int J Solids Struct 49 (17) (2012) 2291–2300.
[33] J.G. Van Mier, Fracture processes of concrete, vol. 12, CRC press, 1996.
[34] P. Folino, G. Etse, Validation of performance-dependent failure criterion for concretes, ACI Mater J 108 (3) (2011).
[35] Caggiano A. Meso-mechanical analysis of steel fiber reinforced cementitious composites, PhD thesis. University of Salerno (Italy) and National University of Tucuman (Argentina), Int. Co-supervised Thesis; 2014.